
This is an electronic reprint of the original article.
This reprint may differ from the original in pagination and typographic detail.

Lin, Huawei; Chen, Quangang; Ji, Yuan; Yang, Xujun; Wang, Jianpeng; Ge, Lei
Weak-Field-Based Self-Decoupling Patch Antennas

Published in:
IEEE Transactions on Antennas and Propagation

DOI:
[10.1109/TAP.2020.2970109](https://doi.org/10.1109/TAP.2020.2970109)

Published: 01/06/2020

Document Version
Peer reviewed version

Please cite the original version:
Lin, H., Chen, Q., Ji, Y., Yang, X., Wang, J., & Ge, L. (2020). Weak-Field-Based Self-Decoupling Patch Antennas. *IEEE Transactions on Antennas and Propagation*, 68(6), 4208-4217. [8979277].
<https://doi.org/10.1109/TAP.2020.2970109>

This material is protected by copyright and other intellectual property rights, and duplication or sale of all or part of any of the repository collections is not permitted, except that material may be duplicated by you for your research use or educational purposes in electronic or print form. You must obtain permission for any other use. Electronic or print copies may not be offered, whether for sale or otherwise to anyone who is not an authorised user.

Weak-Field-Based Self-Decoupling Patch Antennas

Huawei Lin, Quangang Chen, Yuan Ji, Xujun Yang, *Student Member, IEEE*, Jianpeng Wang and Lei Ge, *Senior Member, IEEE*

Abstract—In this paper, a new self-decoupling method, namely weak-field-based decoupling technique, is proposed and validated based on inset-fed patch antenna arrays. The self-decoupling effect is realized by taking advantage of the inherent weak-field area created by the feeding structure and proposed inset-fed patch. By strategically arranging the array element in the weak-field area of the adjacent antenna element, the coupling strength between adjacent elements can be controlled under a very low level without the need of any additional decoupling circuitry or structures. A two-element patch antenna array was first developed and analyzed, achieving a peak isolation level of 61 dB. Afterwards, a four-element linear patch antenna array was designed, fabricated and measured to further validate the proposed technique. With the distinct advantages of simple structure and effective isolation enhancement, the proposed self-decoupling method is very promising for MIMO applications.

Index Terms—Antenna array, patch antenna, multiple input multiple output (MIMO), self-decoupling.

I. INTRODUCTION

WITH the rapid development of wireless communication systems, especially the fifth-generation (5G) mobile communications, multiple input multiple output (MIMO) technique has been widely used to obtain high data transmission rate and large channel capacity [1], [2]. However, one of the most important and urgent problems is electromagnetic interference due to the coupling between MIMO antenna elements, which deteriorates the performance of MIMO systems [3]. Under this circumstance, it is critical and meaningful to find simple and effective decoupling methods for MIMO antenna arrays.

In recent years, several decoupling methods have been reported, including metamaterials, defected ground structures (DGS), parasitic elements, neutralization lines, decoupling networks, etc. Generally, metamaterial structures were used as isolators to block surface or space wave between antennas [4]-[7]. DGS could play a role of band-stop filters to suppress mutual coupling between antenna elements [8], [9]. Additional

coupling paths could be introduced by parasitic elements or other similar elements in order to decrease the coupling [10]-[13]. Parasitic monopoles were reported to improve the isolation of a tri-slot antenna array [10]. An array-antenna decoupling surface was utilized to create reflective electromagnetic waves for cancelling out undesired coupling waves in four-element and eight-element antenna systems [11]. Besides, the coupling between three-port MIMO antennas could be reduced by loading reactive dummy elements [12]. In [13], short-circuited stepped-impedance structures were adopted to improve the isolation in a 2×2 patch antenna array. In order to counteract the undesired coupling, neutralization lines or other circuits were adopted to bridge strongly coupled antennas [14]-[16]. Unlike the direct connection of neutralization lines, decoupling networks were based on coupled resonators or coupled circuitry to achieve high port-to-port isolation [17]-[19]. Nevertheless, both neutralization lines and decoupling networks increase the complexity of the circuitry when the number of antenna elements increases. Although the aforementioned methods show attractive decoupling performance, they suffer from inconvenience and complexity caused by additional decoupling structures.

In order to overcome the shortcomings of the introduced decoupling structures, some novel decoupling methods [20]-[23] have been proposed very recently. These methods decreased mutual coupling without additional decoupling structures. In [20], a self-curing decoupling technique, only requiring the addition of a capacitive load on the antenna elements, was proposed to reduce the mutual coupling between two inverted-F antennas. In [21], a novel pattern-diversity-based method was successfully used to decouple different types of monopole antennas. In [22], high-order modes of a ground plane were studied and used to decouple two inverted-F antennas. Nevertheless, an auxiliary decoupling strip was required when the number of antenna elements extended to three. In [23], a self-isolated antenna was proposed for 5G mobile applications. However, even though the authors made an effort to miniaturize the antenna size, the antenna was still comparatively large.

In this paper, a new self-decoupling method is introduced and validated based on inset-fed microstrip patch antennas. By carefully adjusting the geometry parameters of the feeding structure, the two fields excited by the feeding structure and the patch will cancel each other out and form a weak-field area on the ground plane. Then, weak electromagnetic interference between antenna elements can be realized when arranging the adjacent antenna element in the weak-field area. To verify the feasibility of our proposed scheme, this method is first applied in a two-element antenna array and then extended to a four-

This work was supported in part by the Fundamental Research Foundation of Shenzhen under Grant No. JCYJ20170817095519575 and in part by the Shenzhen Science and Technology Innovation Commission under Grant No. JCYJ20170818093035338. (Corresponding author: Lei Ge.)

H. Lin, Q. Chen, and L. Ge are with the College of Electronic and Information Engineering, Shenzhen University, Shenzhen, China. (e-mail: leige@szu.edu.cn).

X. Yang is with the College of Physics and Optoelectronic Engineering, Shenzhen University, Shenzhen, China.

Y. Ji and J. Wang are with the Ministerial Key Laboratory of JGMT, Nanjing University of Science and Technology, Nanjing 210094, China.

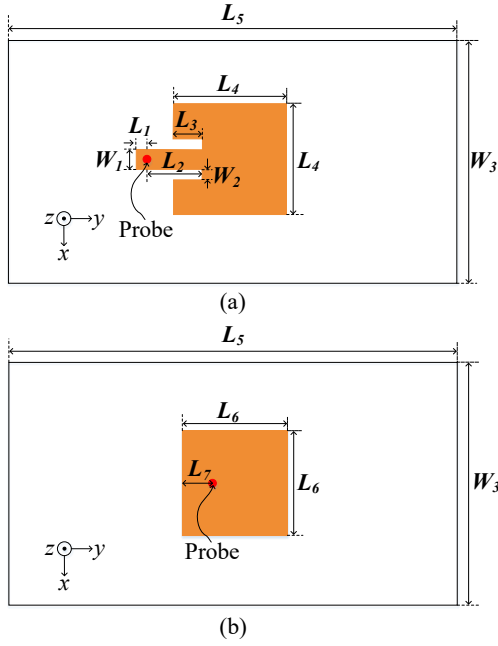


Fig. 1. Geometry of (a) the proposed inset-fed patch antenna element and (b) the reference probe-fed patch antenna element.

element antenna array. Both the simulated and measured results demonstrate that high level port-to-port isolations are realized in the aforementioned arrays. Moreover, the antenna structure is simple, and the implementation of decoupling effect does not demand any additional decoupling circuitry or structures.

The rest of this paper is organized as follows: In Section II, the self-decoupling principle is illustrated. The measurement results and discussion of the proposed method applied in two-element antenna array are provided in Section III. Section IV demonstrates the feasibility of its implementation in a four-element linear antenna array. Finally, a conclusion is given in Section V.

II. WEAK-FIELD-BASED SELF-DECOUPLING MECHANISM

In this section, the basic antenna element is first introduced, and its current distribution, E- and H-field distributions, and equivalent circuit model are utilized to illustrate the self-decoupling mechanism. Then another antenna element is subsequently added to form a two-element array in order to validate the effect of the self-decoupling method. Lastly, key parameters are analyzed to intuitively confirm the proposed self-decoupling principle.

A. Antenna Element

The geometry of the proposed inset-fed patch antenna element is shown in Fig. 1(a). The antenna is built on a substrate with a relative dielectric constant of 2.33 and a thickness of 3.175 mm. The proposed patch antenna is implemented on the top of the substrate and excited by a specific feeding structure. The feeding structure is composed of a microstrip line and a probe. An inset feed is created for the microstrip line to control the variation of the input impedance of the radiating patch. The input impedance of the radiating patch can be approximately calculated by the following equations given in [24].

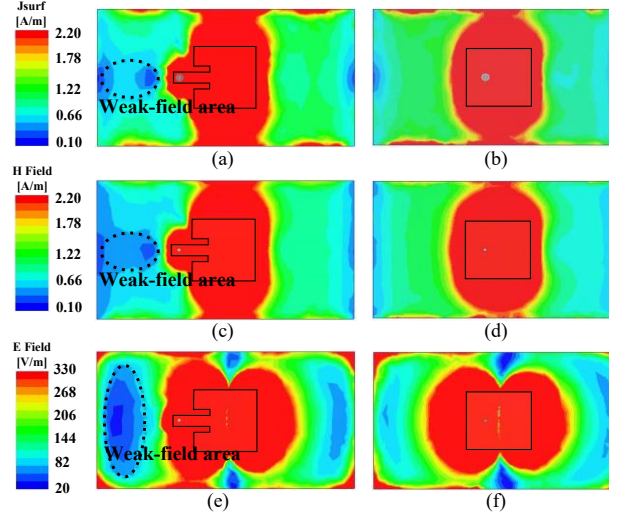


Fig. 2. Surface current distributions on the ground plane of (a) the proposed antenna element and (b) the reference antenna element; H-field distributions over the ground plane of (c) the proposed antenna element and (d) the reference antenna element; E-field distributions over the ground plane of (e) the proposed antenna element and (f) the reference antenna element.

$$R_i = R_e \cos^4 \frac{\pi L_3}{L_4} \quad (1)$$

$$R_e = \frac{1}{2G} \quad (2)$$

$$G = \frac{\pi L_4}{\eta \lambda_0} \left[1 - \frac{(kH)^2}{24} \right] \quad (3)$$

where L_3 and L_4 are the lengths of the slots and the patch, respectively. R_e is the input impedance of the patch when the slot length is zero, which can be calculated from (2) and (3). Based on (3), the conductance G of one side of the patch can be calculated. H is the thickness of the substrate; η represents the impedance of the space wave; k and λ_0 are the wavenumber and wavelength in the free space, respectively.

In order to illustrate the principle and characteristics of the proposed self-decoupling antenna, a conventional probe-fed patch antenna with a structure shown in Fig. 1(b) is given for a comparison. It has the same substrate and ground size with the proposed inset-fed antenna. Moreover, both antennas operate at the same frequency and have nearly identical radiation characteristics. The specific analysis results will be described in detail in the following content.

B. Self-Decoupling Mechanism

To study the self-decoupling mechanism of the proposed inset-fed antenna element, the surface current distributions on the ground plane of the two antennas are simulated and compared in Fig. 2(a) and (b). For the proposed inset-fed patch antenna, a very conspicuous low current density area is formed in the vicinity of the feeding structure, marked by the black elliptical dotted line in Fig. 2(a). While for the reference probe-fed patch antenna, the entire ground plane has a relative strong current distribution, and no weak-field area exists near the patch

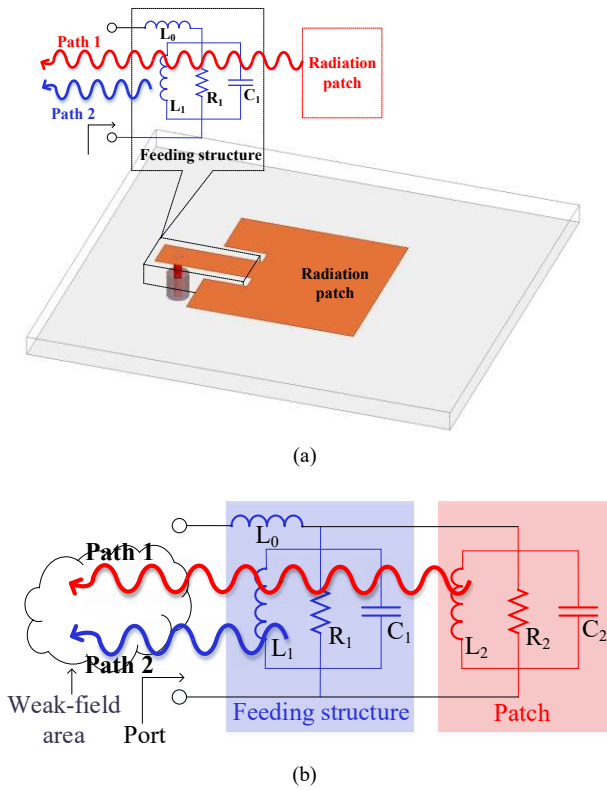


Fig. 3. Over-simplified equivalent circuit models of (a) the proposed feeding structure and (b) the proposed inset-fed antenna element.

TABLE I

DIMENSIONS OF THE TWO-ELEMENT ANTENNA ARRAY

Parameters	L_1	L_2	L_3	L_4	L_5	L_6	L_7
Values/mm	3	13	7	27.3	110	25.62	7.41
Parameters	L_8	L_9	W_1	W_2	W_3	D	D_1
Values/mm	105	17.45	5	2.5	60	42.8	6.5

as shown in Fig. 2(b). Furthermore, the H-field and E-field distributions over the ground plane of the both antennas can also be seen in Fig. 2. There exists a weak H-field region on the port (left) side of the proposed antenna. Likewise, the E-field intensity near the feeding structure of the proposed antenna element is comparatively low.

The arisen weak-field area can be explained through a simplified equivalent circuit model, as shown in Fig. 3. There are mainly two coupling paths near the feeding structure of the proposed antenna. One is Path 1 and its field source is the radiating of the patch, denoted by the red wavy line. The other one is Path 2 formed by the feeding structure, denoted by the blue wavy line. A coaxial probe connects directly to the feeding strip line and it vertically penetrates a reserved through hole of the substrate, as shown in Fig. 3(a). The probe is equivalent to an inductor, and the weakly radiated feeding microstrip line is equivalent to an RLC network. There exists coupling energy between the probe and the feeding strip line along Path 2. The field source of Path 2 is weaker than that of Path 1. Since the magnitude of the coupling field is related to the coupling distance, the coupling fields from Path 1 and Path 2 can be equal in amplitude in the specific weak-field area, where it is near the feeding structure and far away from the patch. In order to realize

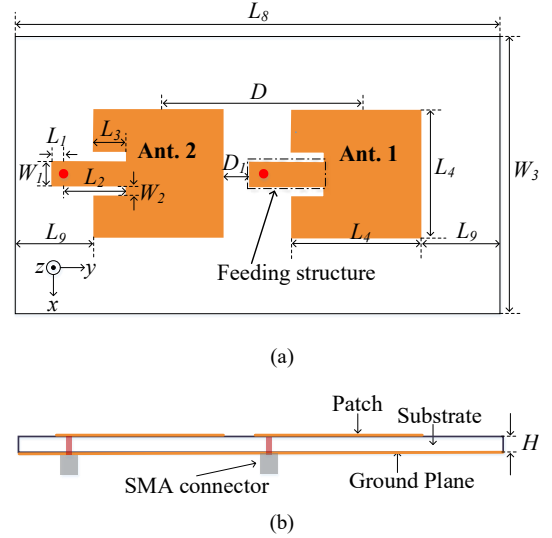


Fig. 4. Geometry of the proposed two-element self-decoupling patch antenna array: (a) top view; (b) side view.

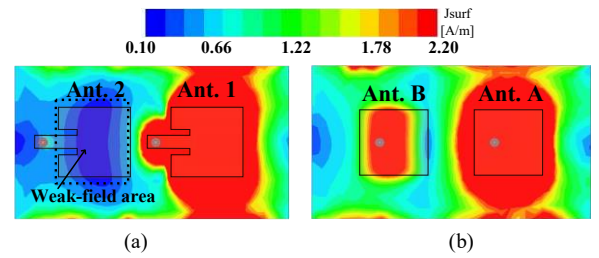


Fig. 5. Surface current distributions on the ground plane of the two-element antenna arrays at 3.5 GHz: (a) the proposed inset-fed antenna array; (b) the reference probe-fed antenna array.

the weak-field area, the coupling fields from the two parts must have opposite phases in addition to equal magnitude. The phase difference of the two coupling fields is affected by two factors. One is the phase difference between two field sources, the other one is the distance difference between Paths 1 and 2. By carefully selecting the dimensions of the feeding structure, the coupling fields from the two paths can be equal in magnitude and opposite in phase simultaneously, thus forming the weak-field area, as illustrated in Fig. 3 (b). Here the interaction between the feeding structure and the radiating patch is omitted on account of the realistic circuit model is very complex and it is difficult to quantitatively calculate the exact values of the circuit parameters. It is predictable that if another antenna element is placed in the weak-field area of the inset-fed antenna element, the coupling strength between the two antennas will be weak.

The geometry of the two-element antenna array is depicted in Fig. 4, where Ant. 2 is exactly the same with Ant. 1. It is worth mentioning that the mutual coupling can be affected by the ground size. The size of the ground plane is fixed at $105 \text{ mm} \times 60 \text{ mm}$ ($1.2\lambda_0 \times 0.7\lambda_0$, where λ_0 is the free-space wavelength at the center operation frequency of 3.5 GHz) here. The thickness of the substrate, H , is 3.175 mm and the relative dielectric constant, ϵ_r , is 2.33. The dimensions are listed in Table I. 50- Ω SMA connectors are employed to feed the antenna elements. Fig. 5 plots the surface current distributions of the proposed

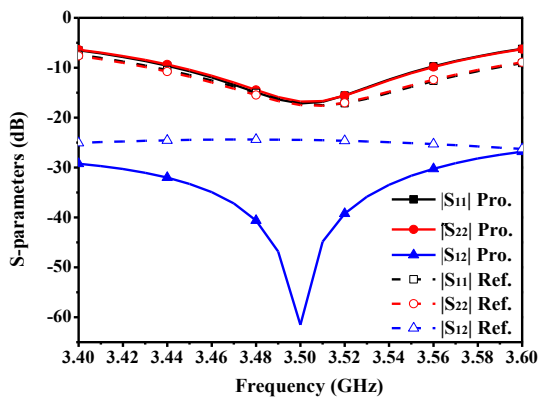


Fig. 6. Simulated S-parameters of the proposed and the reference two-element antenna arrays.

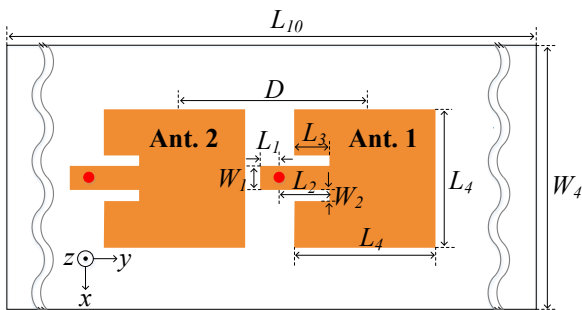


Fig. 7. Parameter description of the proposed two-element antenna array.

inset-fed and the reference probe-fed antenna arrays at 3.5 GHz, where the both arrays are with the same element spacing. When Ant. 1 and Ant. A are excited, Ant. 2 and Ant. B are terminated with 50- Ω loads. For the proposed self-decoupling inset-fed patch antenna array, the current intensity on Ant. 2 is very weak, as indicated by the black rectangle dotted line in Fig. 5(a). However, for the reference probe-fed patch antenna array, the current intensity on Ant. B is strong due to the coupling of Ant. A, as shown in Fig. 5(b).

The simulated S-parameters of the proposed inset-fed patch antenna array and the reference probe-fed antenna array are shown in Fig. 6. The reflection coefficients of the probe-fed antenna elements are designed to be consistent with that of the inset-fed antenna elements. At 3.5 GHz, the reflection coefficients of the antennas in the two arrays are nearly identical and all better than -10 dB. On the other hand, the isolation of the reference probe-fed antenna array is 24 dB, whereas the isolation of the proposed inset-fed antenna array is 61 dB at 3.5 GHz. What's more, an isolation level of more than 30 dB is achieved for the proposed inset-fed antenna array within the impedance band ($|S_{11}| \leq -10$ dB).

C. Parametric Study

Some key parameters are studied by comparing the mutual coupling strength of different array cases to give a design guideline. The parameter description of the antenna arrays is depicted in Fig. 7. Correspondingly, the parameters of the different cases are listed in Table II, and they are designed to operate at 3.5 GHz. The length of the ground plane, L_{10} , is changed to $2.33\lambda_0$ in order to give enough location space for antenna elements when the antenna parameters vary.

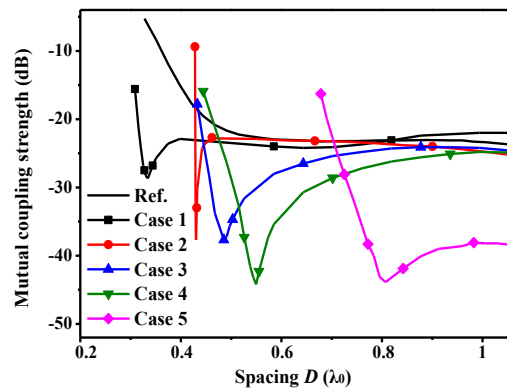


Fig. 8. Coupling strength of the two-element array with varying parameter.

TABLE II
PARAMETER OF DIFFERENT ARRAYS

Case	1	2	3	4	5
ϵ_r	4.4	2.33	2.33	2.33	1
H (mm)	3.175	1	3.175	5	3.175
W_1 (mm)	4	1.4	5	5	4
W_2 (mm)	2	2	2.5	2.5	2
W_4 (mm)	45	60	60	60	80
L_1 (mm)	3	1.8	3	3	6
L_2 (mm)	8.4	15.1	13	13	21
L_3 (mm)	5.7	8	7	6.3	8.6
L_4 (mm)	20.4	27.7	27.3	26.4	39

In Fig. 8, the coupling strength of different array cases versus the antenna spacing D is figured and compared. It can be clearly observed that all the listed inset-fed patch array cases have null point of the coupling strength at different antenna spacings. As a contrast, the coupling strength versus spacing of the aforementioned reference probe-fed patch array is also given in Fig. 8, where no null point emerges on the curve. It should be pointed out that when $\epsilon_r = 2.33$ and $H = 3.175$ mm (Case 3), the null point of the mutual coupling strength occurs at $0.5\lambda_0$, which means this case is the same with the aforementioned array in Section II-B. Yet the coupling strength at 3.5 GHz in Fig. 8 is larger than that of the aforementioned array in Fig. 6, which is due to the size difference of the ground plane. By comparing the coupling strength of Case 1, Case 3 and Case 5, it can be observed that when the substrate thickness is identical, the higher the dielectric constant, the smaller spacing the null point of coupling appears. By comparing Case 2, Case 3 and Case 4 which are with the same dielectric constant, the thicker the substrate is, the larger spacing the null point of coupling strength appears. In addition to the given antenna array cases, designs with different ϵ_r and H can produce different coupling strength curves versus antenna spacing. It means that the proposed self-decoupling method is able to be applied to different array designs which have specific requirements on the antenna spacing.

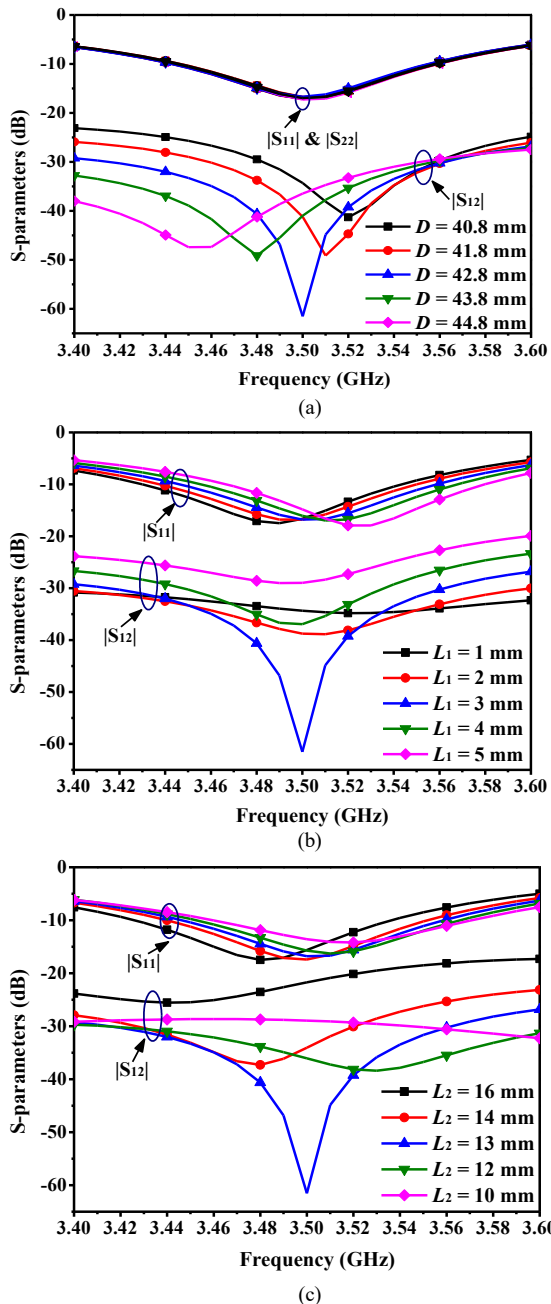


Fig. 9. Simulated S-parameters of the two-element array with (a) different spacing D ; (b) different length L_1 and (c) different length L_2 .

In order to intuitively study the effect of other antenna parameters on the coupling strength. Taking the antenna array built on a substrate with $\epsilon_r = 2.33$ and $H = 3.175$ mm as an example, three critical parameters, namely the spacing D of the antennas, the lengths L_1 and L_2 of the feeding structure are analyzed as follows.

The S-parameters with different D are given in Fig. 9(a). As the figure shows, the reflection coefficient of the antenna element is not affected by D . As D increases from 40.8 mm ($0.477\lambda_0$) to 44.8 mm ($0.523\lambda_0$), the null point of the coupling strength shifts from 3.52 to 3.48 GHz. In Fig. 9(b), when L_1 increases, the resonance frequency of the antenna shifts toward high frequency. The curves of $|S_{11}|$ and $|S_{22}|$ are approximately identical with the change of L_1 , and the curves of $|S_{12}|$ are not

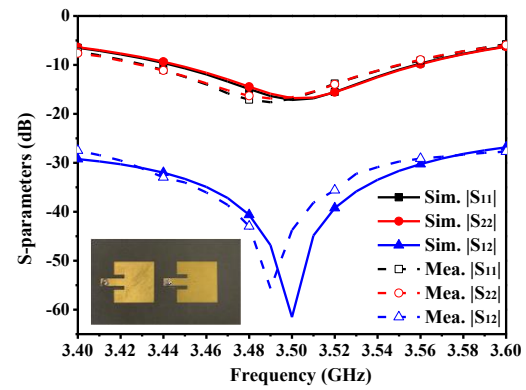


Fig. 10. Simulated and measured S-parameters of the proposed two-element antenna array.

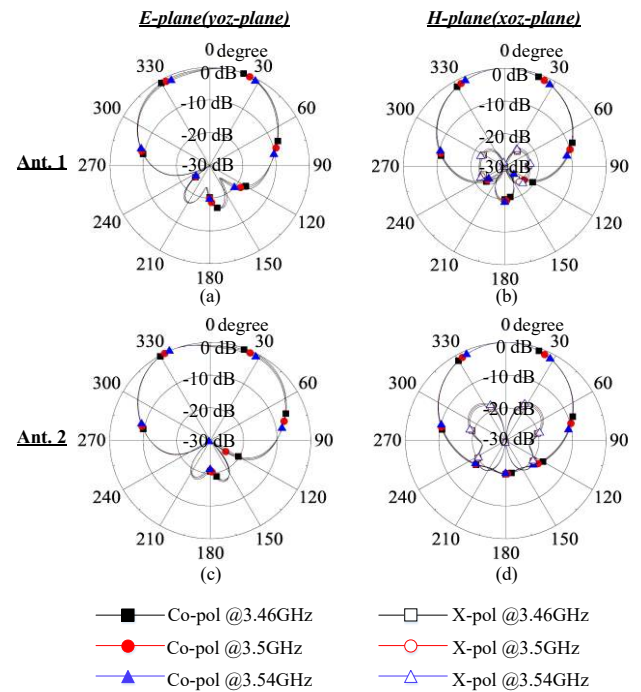


Fig. 11. Simulated radiation patterns of the proposed two-element array at different frequencies: (a) E-plane of Ant. 1; (b) H-plane of Ant. 1; (c) E-plane of Ant. 2; (d) H-plane of Ant. 2.

given for better display effect of the figure. The null point of the coupling strength shifts to higher frequency as L_1 increases. When $L_1 = 3$ mm, the minimum mutual coupling of -61 dB can be achieved. The effect of L_2 on the S-parameters is shown in Fig. 9(c). As L_2 increases, the frequency of the peak isolation and the resonance frequency of the antenna shift toward low frequency. In this design, the microstrip line has characteristic impedance of approximately 74Ω and work as an impedance transformer. So the alteration of L_2 can affect the input impedance of the antenna. The curves of $|S_{11}|$ and $|S_{22}|$ are still approximately identical and the curves of $|S_{22}|$ are not given for the sake of brevity. As observed from the figure, S_{12} is more sensitive to L_2 . When $L_2 = 13$ mm, the isolation of the antenna reaches maximum.

In summary, a high isolation level can be achieved by strategically designing the element spacing and the length of the feeding structure.

TABLE III
A RADIATION PATTERN COMPARISON FOR SINGLE AND DUAL ELEMENTS

Case	Configuration	Peak Gain (dBi)	HPBW (deg)		FTBR (dB)		X-pol level (dB)	
			E-plane	H-plane	E-plane	H-plane	E-plane	H-plane
A	W/o Ant. 2 Ant. 1	7.5	92	77	-20	-19	-48	-22
B	Ant. 2 W/o Ant. 1	7.0	101	78	-20	-20	-49	-17
C	Ant. 2 Ant. 1	7.5	93	77	-20	-19	-54	-23
D	Ant. 2 Ant. 1	7.1	104	77	-21	-20	-53	-16

* HPBW: half-power beamwidth; FTBR: front-to-back ratio; ● excited; ○ terminated with a 50-Ω load.

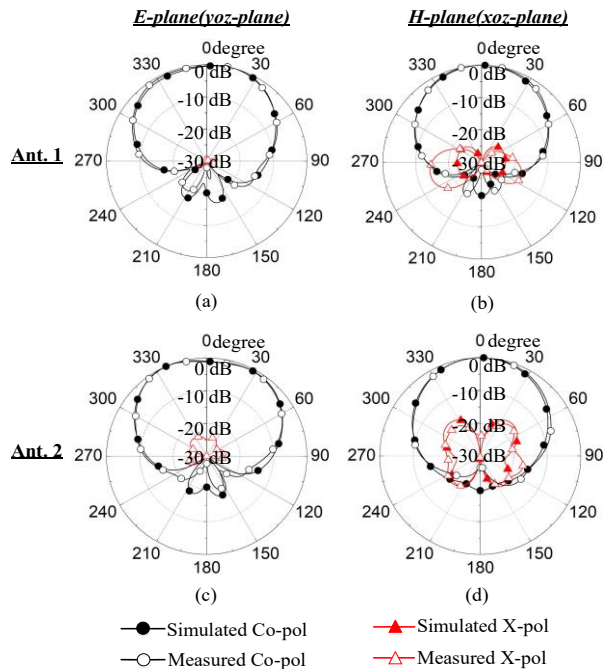


Fig. 12. Simulated and measured radiation patterns of the proposed two-element array at 3.5 GHz: (a) E-plane of Ant. 1; (b) H-plane of Ant. 1; (c) E-plane of Ant. 2; (d) H-plane of Ant. 2.

III. RESULTS AND DISCUSSION

A. Result

The simulated and measured S-parameters of the proposed self-decoupling antenna array are shown in Fig. 10. The slight difference between the measured and the simulated results is owing to fabrication and test tolerances. The coupling strength of the antenna array is too weak and therefore is very sensitive to the test environment.

In order to show that radiation patterns are considerable consistent over the entire band, the simulated patterns of the

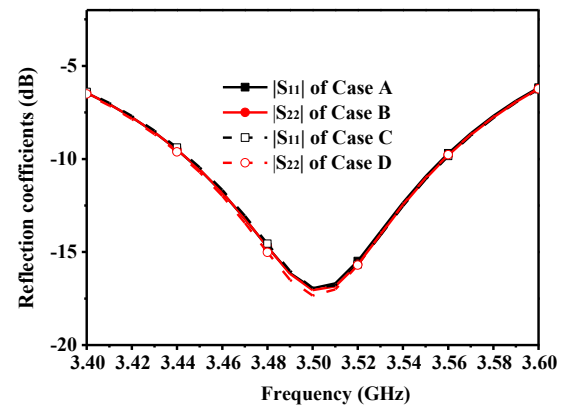


Fig. 13. Simulated reflection coefficients under four different configuration cases.

proposed two-element array at different frequencies are given in Fig. 11, which are in line with expectations. And the simulated and measured radiation patterns of the two-element array at 3.5 GHz are plotted in Fig. 12. The radiation pattern of Ant. 1 or Ant. 2 was measured separately while the other antenna port was matched. It can be found that the E-plane radiation patterns of Ant. 1 and Ant. 2 have a slight variation due to the respective different locations on the ground plane. Besides, stable H-plane radiation patterns can be obtained.

B. Discussion

On purpose of studying the mutual influence between antenna elements, we list four different antenna configuration cases, as illustrated in the second column of Table III. The solid red circle represents the antenna element is excited, whereas the hollow black circle denotes it is terminated with a 50-Ω load. The simulated reflection coefficients of these cases are given in Fig. 13, and the corresponding radiation patterns at 3.5 GHz are shown in Fig. 14. Besides, a summarization of all these patterns is tabulated in Table III for clarity.

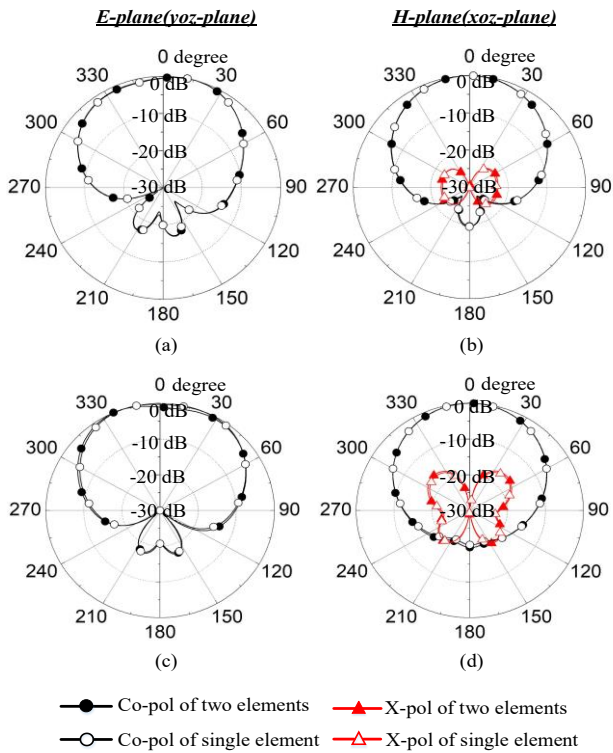


Fig. 14. Simulated radiation patterns under four different configuration cases at 3.5GHz: (a) E-plane of Cases A and C; (b) H-plane of Cases A and C; (c) E-plane of Cases B and D; (d) H-plane of Cases B and D.

More specifically, the performances of Ant. 1 without and with Ant. 2 are compared to show the influence of Ant. 2 on Ant. 1, and the corresponding configurations are named Cases A and C, respectively. Similarly, Cases B and D are compared to show the effect of Ant. 1 on Ant. 2. From Fig. 13, the curves of reflection coefficients of the antenna element in the four cases agree well. Therefore, under these circumstances, the proposed decoupling method has no distinct impact on the bandwidth.

With respect to the impact on radiation patterns, let's first look at the cases A and B, which are both situations of the single antenna element. It can be found that the E-plane (yoz-plane) half-power beamwidth (HPBW) of Case A is comparatively smaller than that of Case B, whereas the H-plane HPBWs are basically consistent. This is attributed to the weak-field area introduced by the proposed inset-fed structure of Ant.1 is situated on its left side (i.e., along the negative y-axis direction), so it reduces radiation from the induced current on the ground plane of Case A, resulting in a higher broadside gain and a narrower HPBW in the E-plane than that of Case B.

Notably, when we contrast the case A with C, the difference between the two cases is that whether we place Ant. 2 in the weak-field area close to the feeding structure of the excited element Ant. 1. As can be seen in Fig. 14(a) and (b), it is concluded that the proposed decoupling method has high preservability of radiation patterns under the given condition. With reference to the cases B and D, a slight variation of E-plane radiation patterns can be found on the condition that whether we place Ant. 1 in the non-weak-field area of the excited element Ant. 2, as shown in Fig. 14(c) and (d). It should

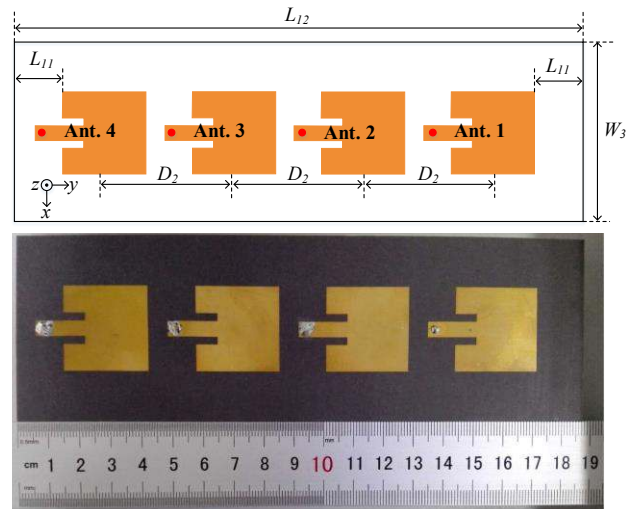


Fig. 15. Geometry and fabricated prototype of the four-element linear array.

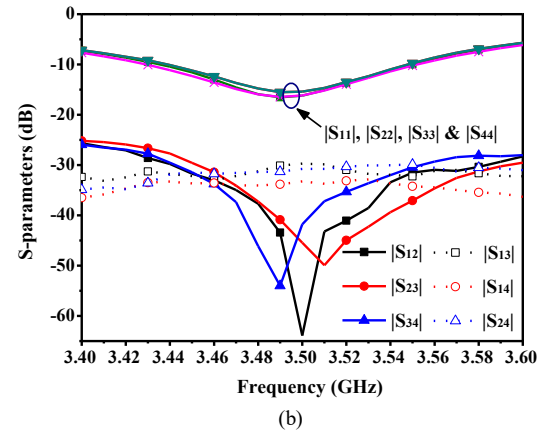
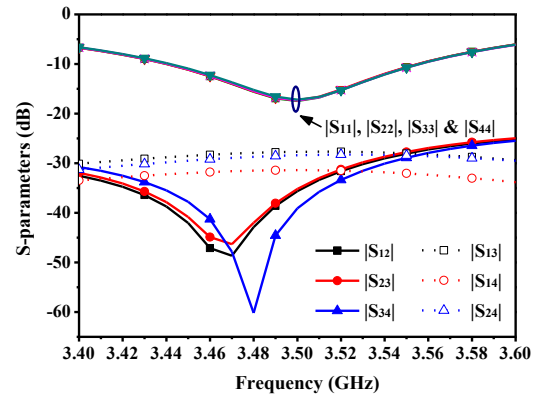
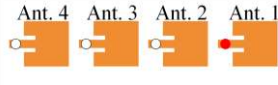
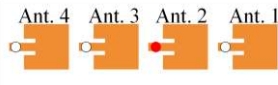

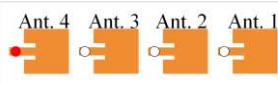


Fig. 16. S-parameter results of the four-element linear array: (a) simulation; (b) measurement.

be pointed out since the coupling power level is mostly low, the minimization of coupling caused by self-decoupling method is low and introduces small influence on radiation patterns and impedance matching.

In addition, the cross-polarization levels in the H-plane are higher than that in the E-plane. We can find the H-plane cross-polarization basically remains unchanged between the two

TABLE IV
A RADIATION PATTERN COMPARISON FOR FOUR ELEMENTS

Configuration	Peak Gain (dBi)	HPBW (deg)		FTBR (dB)		X-pol level (dB)	
		E-plane	H-plane	E-plane	H-plane	E-plane	H-plane
	7.6	98	77	-22	-21	-45	-22
	6.9	121	82	-18	-17	-45	-17
	6.7	124	79	-18	-18	-47	-21
	7.1	117	75	-26	-25	-48	-17

* HPBW: half-power beamwidth; FTBR: front-to-back ratio; ● excited; ○ terminated with a 50-Ω load.

cases A and C (or the two cases B and D). That is to say, the cross polarization is principally generated by the inset-fed patch antenna element itself but not the decoupling method.

IV. SELF-DECOUPLING FOUR-ELEMENT ANTENNA ARRAY

In this section, a four-element antenna array is designed based on the aforementioned self-decoupling method. The geometry of the four-element antenna array, as well as the photo of the fabricated prototype, is shown in Fig. 15. The four antenna elements are with the same size and the element spacing is 42.8 mm ($0.5\lambda_0$). The array is also printed on the same substrate with $H = 3.175$ mm and $\epsilon_r = 2.33$. The dimensions of the single antenna element in the array are identical to that in the aforementioned two-element array given in Section II-B. Only the size of the ground plane is enlarged to 60 mm × 188 mm.

The simulated S-parameters of the four-element patch antenna array are shown in Fig. 16(a). The differences between $|S_{11}|$, $|S_{22}|$, $|S_{33}|$ and $|S_{44}|$ are subtle over the -10 dB impedance band from 3.45 to 3.55 GHz. It is worth mentioning that the four antennas are not placed symmetrically but arranged linearly, so the antenna elements in the array have different electromagnetic environment. However, the reflection coefficients of all the elements are almost the same, indicating that the proposed four-element array has no distinct impact on the impedance matching.

For adjacent antennas, the values of $|S_{12}|$, $|S_{23}|$ and $|S_{34}|$ are all less than -29 dB over the band from 3.45 to 3.55 GHz, among which the null point of coupling strength between adjacent antennas appears at 3.47, 3.47 and 3.48 GHz, respectively. While for non-adjacent antennas, high isolation of more than 28 dB is achieved due to the large spacing between them. As shown in Fig. 16(b), the measured S-parameters are slightly different from the simulated values, which may result from manufacturing and test tolerance. Both simulated and measured results show excellent isolation performance.

The simulated and measured radiation patterns of the four-element array at 3.5 GHz are plotted in Fig. 17. Besides, based on the simulated radiation patterns at different frequencies, all

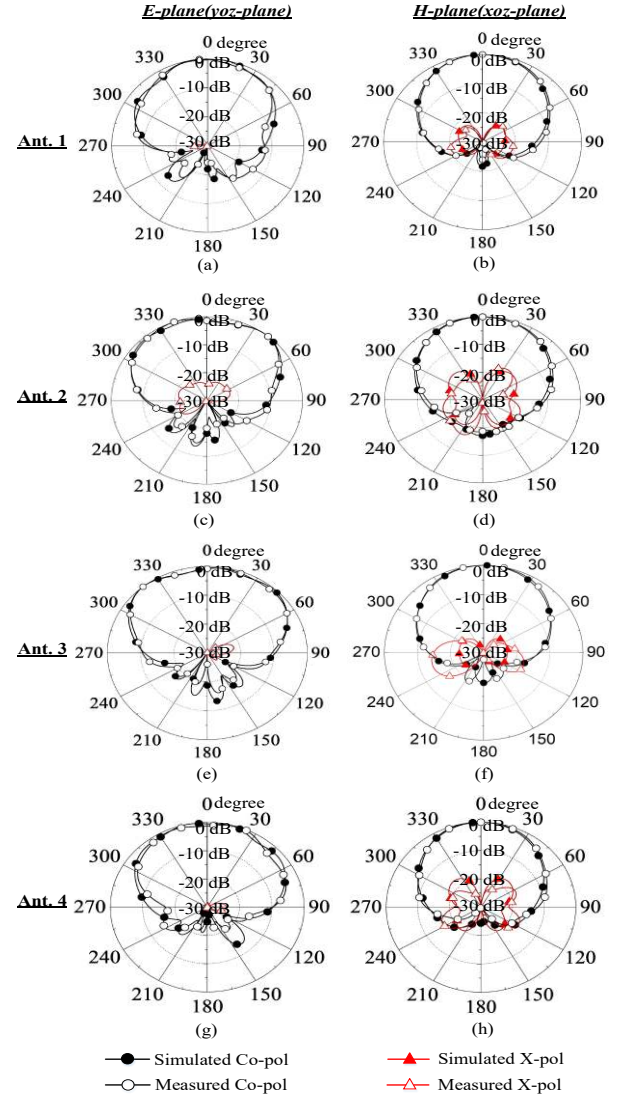


Fig. 17. Simulated and measured radiation patterns of the four-element linear array at 3.5GHz: (a) E-plane of Ant. 1; (b) H-plane of Ant. 1; (c) E-plane of Ant. 2; (d) H-plane of Ant. 2; (e) E-plane of Ant.3; (f) H-plane of Ant.3; (g) E-plane of Ant.4; (h) H-plane of Ant.4.

the patterns are fairly consistent over the entire band. For comparison, Table IV summarizes the radiation performance of the four elements with one of them successively excited from right to left. When the rightmost Ant. 1 is excited, it presents the best decoupling level as the weak-field area covers the maximal left part proportion of the array. Thus it exhibits the highest gain, the narrowest beamwidth, and the lowest H-plane cross-polarization level in contrast to other circumstances. On the other hand, the E-plane HPBW has fatter beamwidth and smaller gain when we feed Ant. 2, Ant. 3, and Ant. 4. The disparity in the E-plane HPBW between Ant. 1 and Ants. 2-4 is mainly caused by the ground plane. Furthermore, in view of the radiation patterns just discussed, are much alike with those of a single antenna element in different locations on the same ground plane, therefore, the four kinds of single element cases are omitted here for brevity.

All the simulated S-parameters, current distribution, E- and H-field distributions, and radiation patterns in this paper are calculated by software *Ansys HFSS*. The measured S-parameters are carried out by *Keysight N5225A* network analyzer, and the measured radiation patterns are accomplished by a near-field measurement system.

V. CONCLUSION

In this paper, the weak-field-based self-decoupling technique is proposed for the first time. The self-decoupling mechanism takes advantage of the weak-field area formed by the feeding structure and radiating patch of the inset-fed patch antenna. High isolation is demonstrated by a two-element antenna array at first, and then further validated in a four-element array. Importantly, the proposed decoupling method does not require any additional circuitry or structures. With all these advantages, the proposed self-decoupling technique is promising to be applied in MIMO antenna systems.

ACKNOWLEDGEMENT

The authors would like to thank those who personally reviewed the paper and provided their useful comments. Also, they would like to thank the reviewers for giving us their valuable comments.

REFERENCES

- [1] J. G. Andrews et al., "What Will 5G Be?," *IEEE J. Sel. Areas Commun.*, vol. 32, no. 6, pp. 1065-1082, Jun. 2014.
- [2] A. Gupta and R. K. Jha, "A Survey of 5G Network: Architecture and Emerging Technologies," *IEEE Access*, vol. 3, pp. 1206-1232, 2015.
- [3] B. Wang, Y. Chang, and Y. Sun, "Performance of the Large-Scale Adaptive Array Antennas in the Presence of Mutual Coupling," *IEEE Trans. Antennas Propag.*, vol. 64, no. 6, pp. 2236-2245, Jun. 2016.
- [4] C. Hsu, K. Lin, and H. Su, "Implementation of Broadband Isolator Using Metamaterial-Inspired Resonators and a T-Shaped Branch for MIMO Antennas," *IEEE Trans. Antennas Propag.*, vol. 59, no. 10, pp. 3936-3939, Oct. 2011.
- [5] J. Y. Lee, S. H. Kim, and J. H. Jang, "Reduction of Mutual Coupling in Planar Multiple Antenna by Using 1-D EBG and SRR Structures," *IEEE Trans. Antennas Propag.*, vol. 63, no. 9, pp. 4194-4198, Sep. 2015.
- [6] D. A. Ketzaki and T. V. Yioultis, "Metamaterial-Based Design of Planar Compact MIMO Monopoles," *IEEE Trans. Antennas Propag.*, vol. 61, no. 5, pp. 2758-2766, May 2013.
- [7] G. Zhai, Z. N. Chen, and X. Qing, "Enhanced Isolation of a Closely Spaced Four-Element MIMO Antenna System Using Metamaterial Mushroom," *IEEE Trans. Antennas Propag.*, vol. 63, no. 8, pp. 3362-3370, Aug. 2015.
- [8] C. Chiu, C. Cheng, R. D. Murch, and C. R. Rowell, "Reduction of Mutual Coupling Between Closely-Packed Antenna Elements," *IEEE Trans. Antennas Propag.*, vol. 55, no. 6, pp. 1732-1738, Jun. 2007.
- [9] S. Zhang, S. N. Khan, and S. He, "Reducing Mutual Coupling for an Extremely Closely-Packed Tunable Dual-Element PIFA Array Through a Resonant Slot Antenna Formed In-Between," *IEEE Trans. Antennas Propag.*, vol. 58, no. 8, pp. 2771-2776, Aug. 2010.
- [10] Z. Li, Z. Du, M. Takahashi, K. Saito, and K. Ito, "Reducing Mutual Coupling of MIMO Antennas with Parasitic Elements for Mobile Terminals," *IEEE Trans. Antennas Propag.*, vol. 60, no. 2, pp. 473-481, Feb. 2012.
- [11] K. Wu, C. Wei, X. Mei, and Z. Zhang, "Array-Antenna Decoupling Surface," *IEEE Trans. Antennas Propag.*, vol. 65, no. 12, pp. 6728-6738, Dec. 2017.
- [12] J. Deng, J. Li, and L. Guo, "Decoupling of a Three-Port MIMO Antenna with Different Impedances Using Reactively Loaded Dummy Elements," *IEEE Antennas Wireless Propag. Lett.*, vol. 17, pp. 430-433, 2018.
- [13] K. D. Xu, J. Zhu, S. Liao, and Q. Xue, "Wideband Patch Antenna Using Multiple Parasitic Patches and Its Array Application with Mutual Coupling Reduction," *IEEE Access*, vol. 6, pp. 42497-42506, 2018.
- [14] C. Xue, X. Y. Zhang, Y. F. Cao, Z. Hou, and C. F. Ding, "MIMO Antenna Using Hybrid Electric and Magnetic Coupling for Isolation Enhancement," *IEEE Trans. Antennas Propag.*, vol. 65, no. 10, pp. 5162-5170, Oct. 2017.
- [15] A. Diallo, C. Luxey, P. Le Thuc, R. Staraj, and G. Kossiavas, "Study and Reduction of the Mutual Coupling Between Two Mobile Phone PIFAs Operating in the DCS1800 and UMTS Bands," *IEEE Trans. Antennas Propag.*, vol. 54, no. 11, pp. 3063-3074, Nov. 2006.
- [16] A. Cihangir, F. Ferrero, G. Jacquemod, P. Brachat, and C. Luxey, "Neutralized Coupling Elements for MIMO Operation in 4G Mobile Terminals," *IEEE Antennas Wireless Propag. Lett.*, vol. 13, pp. 141-144, 2014.
- [17] L. Zhao, L. K. Yeung, and K. Wu, "A Coupled Resonator Decoupling Network for Two-Element Compact Antenna Arrays in Mobile Terminals," *IEEE Trans. Antennas Propag.*, vol. 62, no. 5, pp. 2767-2776, May 2014.
- [18] L. Zhao and K. L. Wu, "A Dual-Band Coupled Resonator Decoupling Network for Two Coupled Antennas," *IEEE Trans. Antennas Propag.*, vol. 63, no. 7, pp. 2843-2850, Jul. 2015.
- [19] H. Makimura, K. Nishimoto, T. Yanagi, T. Fukasawa, and H. Miyashita, "Novel Decoupling Concept for Strongly Coupled Frequency-Dependent Antenna Arrays," *IEEE Trans. Antennas Propag.*, vol. 65, no. 10, pp. 5147-5154, Oct. 2017.
- [20] J. Sui and K. L. Wu, "Self-Curing Decoupling Technique for Two Inverted-F Antennas with Capacitive Loads," *IEEE Trans. Antennas Propag.*, vol. 66, no. 3, pp. 1093-1101, Mar. 2018.
- [21] C. F. Ding, X. Y. Zhang, C. D. Xue, and C. Y. D. Sim, "Novel Pattern-Diversity-Based Decoupling Method and Its Application to Multielement MIMO Antenna," *IEEE Trans. Antennas Propag.*, vol. 66, no. 10, pp. 4976-4985, Oct. 2018.
- [22] X. Zhao, S. P. Yeo, and L. C. Ong, "Decoupling of Inverted-F Antennas with High-Order Modes of Ground Plane for 5G Mobile MIMO Platform," *IEEE Trans. Antennas Propag.*, vol. 66, no. 9, pp. 4485-4495, Sep. 2018.
- [23] A. Zhao and Z. Ren, "Size Reduction of Self-Isolated MIMO Antenna System for 5G Mobile Phone Applications," *IEEE Antennas Wireless Propag. Lett.*, vol. 18, pp. 152-156, 2019.
- [24] T. A. Milligan, *Modern Antenna Design*, 2nd ed. Hoboken, NJ, USA: John Wiley, 2005, pp.300-324.



Huawei Lin was born in Yunnan, China, in 1994. He received the B.S. degree in optoelectronic information science and engineering from Shenzhen University, China, in 2017. Currently, he is working towards M.S. degree at Shenzhen University. His research interests include patch antennas, MIMO antennas, and the decoupling of MIMO antennas.



Quangang Chen was born in Henan, China, in 1992. He received the B.S. degree in electronic information engineering and M.S. degree in electromagnetic field and microwave technology from the Nanjing University of Science and Technology, Nanjing, China, in 2015 and 2018, respectively. He is currently a Research Assistant with the College of Electronic Science and Technology, Shenzhen University.

His current research interests include multiband smartphone antennas, MIMO antennas and

microwave components.



Yuan Ji was born in Jiangsu, China. She received the B.S. degree in information engineering from the Southeast University, Nanjing, China, in 2009, and the M.S. degree in telecommunication engineering from the University of Melbourne, Melbourne, VIC, Australia, in 2011. She is currently pursuing the Ph.D. degree in electronic science and technology from the Nanjing University of Science and Technology, Nanjing, China.

Her current research interests include phased

arrays and reconfigurable antennas.



XUJUN YANG was born in Lu'an, Anhui, China, in 1993. He received the B.S. degree in applied physics from the Fuyang Normal College, China, in 2016, and the M.S. degree from Shenzhen University in 2018, where he is currently pursuing the Ph.D. degree.

His research interests include base station antennas, reconfigurable antennas, and millimeter-wave antennas.

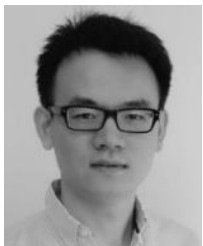


Jianpeng Wang received the Ph.D. degree from the University of Electronic Science and Technology of China, Chengdu, China, in 2007.

From 2005 to 2006, he was a Research Assistant with the Institute for Infocomm Research, Singapore. From 2010 to 2011, he was a Research Fellow with the School of Electrical and Electronic Engineering, Nanyang Technological University, Singapore. In 2013, he joined the School of Engineering and Physical Sciences, Heriot-Watt University, Edinburgh, U.K., as a Visiting Scholar. In

2014 and 2016, he was a Research Fellow with the Faculty of Science and Technology, University of Macau, Macau SAR, China. He is currently an Associate Professor with the School of Electronic and Optical Engineering, Nanjing University of Science and Technology, Nanjing, China. He has authored or co-authored over 90 papers in international journals and conference proceedings. His current research interests include microwave circuits, antennas, and LTCC-based millimeter-wave circuits.

Dr. Wang has been an Associate Editor of IET Electronics Letters since 2015.



Lei Ge (S'11–M'15) was born in Jiangsu, China. He received the B.S. degree in electronic engineering from the Nanjing University of Science and Technology, Nanjing, China, in 2009, and the Ph.D. degree in electronic engineering from the City University of Hong Kong, Hong Kong, in 2015.

From 2010 to 2011, he was a Research Assistant with the City University of Hong Kong. In 2015, he was a Post-Doctoral Research Fellow at the State Key Laboratory of Millimeter Waves, City University of

Hong Kong. He is currently an Assistant Professor and the Associate Head with

the Department of Electronic Engineering, Shenzhen University, Shenzhen, China. His current research interests include wideband antennas, patch antennas, base station antennas, reconfigurable antennas, the antennas for cognitive radio, and filtering antennas.

Dr. Ge was a recipient of the Honorable Mention at the student contest of 2012 IEEE APS-URSI Conference and Exhibition held in Chicago, IL, USA, and the first prize in the Student Innovation Competition of the 2014 IEEE International Workshop on Electromagnetics (IEEE iWEM) held in Sapporo, Japan, in 2014. He was the Session Chair of the iWEM 2017 and ACES-China 2017. He was the TPC Member of the APCAP 2016.